Improved photocatalytic CO_2 and epoxides cycloaddition via the synergistic effect of Lewis acidity and charge separation over Zn modified UiO-bpydc

Guangyao Zhai [a], Yuanyuan Liu [a],[*], Yuyin Mao [a], Honggang Zhang [a], Lingtong Lin [a], Yujie Li [a], Zeyan Wang [a], Hefeng Cheng [a], Peng Wang [a], Zhaoke Zheng [a], Ying Dai [b], Baibiao Huang [a],[*]

[a] State Key Laboratory of Crystal Materials, Shandong University, Jinan 250100, China
[b] School of Physics, Shandong University, Jinan 250100, China

ARTICLE INFO

ABSTRACT

CO_2 cycloaddition reaction from propylene oxide and CO_2 to cyclic carbonates is a desirable process to become carbon neutral. Photo energy can decrease the temperature and pressure needed for this reaction according to our previous results. However, the relationship between Lewis acidity and the photophysical process needs to be clarified and optimized. Hence, in this work, Zn is introduced into UiO-bpydc via the coordination of Zn with the bipyridyl group in bpydc. It is found that the introduction of Zn not only effectively activate propylene oxide, but also promote ligand to metal charge transfer (LMCT) process, which ultimately is beneficial for CO_2 activation. However, Ce plays a negative effect under light irradiation. namely, the presence of Ce facilitates the energy transfer process rather than the LMCT process.

1. Introduction

Annual global CO_2 emission is around 36 billion tons, while the utilization is below 1% in chemical industry. Hence, to be carbon neutral, exploring efficient paths to transform CO_2 into useful chemical products is urgent [1–6]. The CO_2 cycloaddition reaction from CO_2 and propylene oxide (PO) to cyclic carbonate can help to mitigate CO_2 emission, which provides a method to turn the greenhouse gas into high value-added products [7–11]. Cyclic carbonates are widely used as polar solvent, electrolyte of high-density battery, intermediates in some organic reactions and in the synthesis of phenolic resin [12,13]. However, the CO_2 cycloaddition reaction always occur under harsh conditions (high pressure and high temperature), which needs lots of energy and is not economic effective [14,15]. Hence, it is urgent to find a green way to enable the CO_2 cycloaddition reaction occur under mild conditions.

In our previous work [16], light was introduced into above reaction taking advantage that the catalyst (Bi-PCN-224) can also be regarded as semiconductor. The photogenerated electrons produced over Bi-PCN-224 can effectively activate CO_2 under mild conditions, which lowers the energy barrier of this reaction. According to the proposed mechanism, activation of CO_2 and propylene oxide proceed on different sites. The CO_2 activation is tied to photogenerated electrons, and more

efficient charge separation means that more CO_2 molecules are activated. Meanwhile, the propylene oxide activation is mainly related to the Lewis acidity of the catalyst. Therefore, metal with high Lewis acidity (such as Co, Al etc.) are usually preferred [17–19], which however, not certainly leads to high charge separation efficiency. Therefore, it is reasonable to assume that there is a synergistic effect between the two parameters.

To justify above assumption, a Zr based metal organic framework (denoted as UiO-bpydc) containing 2,2′-bipyridine-5,5′-dicarboxylic acid (bpydc) as the organic ligand was chosen as the photocatalyst. The strong coordination ability of bipyridyl in bpydc with metal ions provides a good opportunity to modify the composition of UiO-bpydc (the metal modified sample is denoted as UiO-bpydc(M)) by a post modification process. By adjusting M as the only variable, it is easy to optimize the synergistic effect between Lewis acidity and charge separation efficiency. It is found that the introduction of Zn promotes the CO_2 cycloaddition efficiency, while Ce displays a negative effect. Detailed reasons were investigated with respect to the two processes mentioned above. This work proves that both the Lewis acidity and the photogenerated charge separation efficiency should be considered to achieve an optimal efficiency, which may provide guidance for further designing efficient photocatalysts for CO_2 cycloaddition.

* Corresponding authors.
  E-mail addresses: yyliu@sdu.edu.cn (Y. Liu), bbhuang@sdu.edu.cn (B. Huang).

2. Experimental

2.1. Materials

All reagents were of analytical grade and used without further purification. $ZrCl_4$, $ZnCl_2$, $(NH_4)_2Ce(NO_3)_6$, benzoic acid, 2,2′-bipyridine-5,5′-dicarboxylic acid, propylene oxide, tetrabutylammonium bromide (TBAB) and N-methylacridone were purchased from Aladdin. N,N-Dimethylformamide and concentrated hydrochloric acid (36 wt%−38 wt%) were purchased from Sinopharm Chemical Reagent Co.

2.2. Characterizations

The crystal structure of UiO-bpydc and UiO-bpydc(M) were detected by X-ray power diffractometer (Bruker AXS D8 diffractometer). The composition and element chemical state were analyzed by X-ray photoelectron spectroscopy (Thermo Fisher Scientific Escalab 250 spectrometer). The characteristic functional group of the samples and the coordination environment of metal (Zn or Ce) were detected by Fourier transform infrared spectrometer (Tensor II). N_2 and CO_2 adsorption curves and Brunner−Emmet−Teller surface area were detected by a Micromeritics analyzer (ASAP 2020). The UV–vis diffuse reflectance spectra were detected by Shimadzu UV-2550, $BaSO_4$ used as the substrate. The photoluminescence spectra and NMA fluorescence spectra were obtained by F-4500 FL Spectrophotometer. Electron paramagnetic resonance measurements to detect Zr^{3+} signals were carried on a Bruker A300 spectrometer. Quantitative and qualitative analysis on products and reactants were carried by gas chromatography-mass spectrometry (GC-MS-QP2010, SH-Rtx-Wax column).

2.3. Synthesis of UiO-bpydc

$ZrCl_4$ (120 mg), HCl (360 mg) and benzoic acid (1256 mg) were dissolved in 20 ml DMF solution, After the chemicals were totally dissolved, the H_2bpydc (120 mg) was poured into the above solution which was stirred for 30 min at room temperature. Then the mixture was transferred to Teflon-lined autoclave and heated at 393 K for 24 h in an oven. When the solution was cooled to room temperature, the precipitate was filtered under vacuum and washed several times by acetone and DMF. Finally, the sample UiO-bpydc was dried at 333 K in an oven under vacuum for 12 h.

2.4. Synthesis of UiO-bpydc(Zn)

UiO-bpydc (50 mg) and $ZnCl_2$ (50 mg) were dissolved in 6 ml DMF. After mixture was stirred for 30 mintues, the mixture was transferred to a round bottom flask. Then the solution was heated to reflux at 373 K for 6 h under nitrogen atmosphere. When the solution was cooled down to room temperature, the precipitate was washed several times by acetone and DMF. Finally, the sample UiO-bpydc(Zn) was dried at 333 K in an oven under vacuum for 12 h.

2.5. Synthesis of UiO-bpydc(Ce)

The procedures were the same as that for UiO-bpydc(Zn), except that $ZnCl_2$ was replaced by $Ce(NH_4)_2(NO_3)_6$.

2.6. Electron spin resonance trapping measurement

Each catalyst (4 mg) was loaded into a quartz glass tube. The glass tube was filled with N_2 gas to remove O_2 gas. Then the sample was illuminated by a xenon lamp (300 W 18 A) at 90 K. After that, an amount of CO_2 gas and a dose of propylene oxide were injected into glass tube in order. Free radical signal (Zr^{3+}) was detected by the electron paramagnetic resonance (Bruker A300 spectrometer with a microwave power of 8 mW).

2.7. Fluorescence spectra of N-methylacridone in the presence of samples

10 mg photocatalyst was dispersed in 4 ml MeCN containing NMA with a concentration of 10 mol L^{-1}. Then the suspension was poured into quartz cuvette, which was bubbled with N_2 atmosphere to remove O_2. After that, the suspension was illuminated by a xenon lamp (300 W 18 A) for 10 min. Finally, the fluorescence spectra of the mixed solution were immediately detected by a F-4500 FL Spectrophotometer, with an excitation wavelength of 413 nm.

2.8. Photocatalytic reaction measurement

0.5 mmol co-catalyst (TBAB) and 20 mg catalyst were mixed in a small sealed quartz reactor. Before the propylene oxide was injected into the reactor, the CO_2 gas was bubbled into the glass reactor for 20 min. Then the mixture was irradiated by a xenon lamp (300 W 18 A) and the reaction temperature was maintained at 298 K through the water circulating system. After the reaction, the solution was extracted by a mixed solution containing ethyl acetate and deionized water (volume ratio 1:1). Then GC-MS was used to detect the unreacted propylene oxide and cyclic carbonate qualitatively and quantitatively. Ar was used as carrier gas.
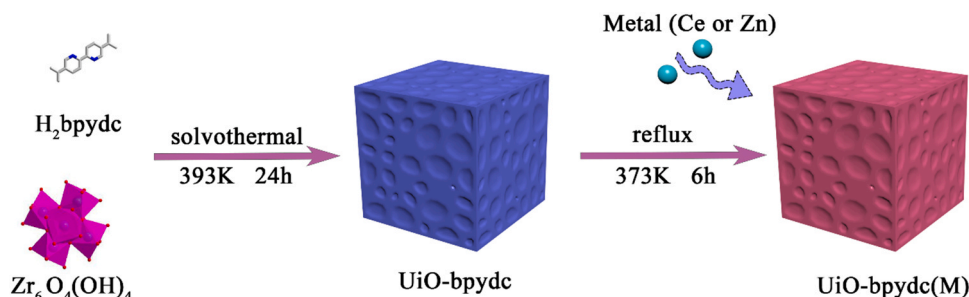
2.9. Theoretical calculations

The first principles were employed to perform density functional theory (DFT) calculations within the generalized gradient approximation (GGA) using the Perdew-Burke-Ernzerhof (PBE) formulation. [20–22] Projected augmented wave (PAW) potentials were chosen to describe the ionic cores and the valence electrons were considered using a plane wave basis set with a kinetic energy cutoff of 450 eV. Partial occupancies of the Kohn−Sham orbitals were allowed using the Gaussian smearing method and a width of 0.05 eV.[23,24] The electronic energy was considered self-consistent when the energy change was smaller than 10^{-5} eV. A geometry optimization was considered convergent when the energy change was smaller than 0.03 eV Å^{-1}. For Zr atoms, the U applied with 3.12 eV. Grimme's DFT-D3 methodology was used to describe the dispersion interactions among all the atoms in the adsorption models.[25] In our calculation, the spin correction was used. The adsorption energies(E_{ads}) were calculated as $E_{ads}= E_{ad/sub}$ -E_{ad} -E_{sub}, where $E_{ad/sub}$, E_{ad}, and E_{sub} were the total energies of the optimized adsorbate/substrate system, the adsorbate in the structure, and the clean substrate, respectively.

3. Results and discussion

3.1. Characterization

UiO-bpydc(M) was synthesized by two steps (Scheme 1). Firstly, the UiO-bpydc was prepared by a solvothermal method [26]. Secondly, metal ions (Zn or Ce) were introduced into UiO-bpydc by a reflux method, and the obtained sample was denoted as UiO-bpydc(M), in which metal coordinates with the bipyridyl in H_2bpydc. The X-ray diffraction (XRD) spectra of the samples (Fig. 1a) show the characteristic peaks of UiO-bpydc, which are consistent with that previously reported [27,28]. Notably, the peaks for metallic oxide or metal hydroxide cannot be observed, which means the introduced Zn (II) or Ce (IV) hardly changes the crystal structure of UiO-bpydc. In other words, the crystal structure of UiO-bpydc is retained for UiO-bpydc(Zn) or UiO-bpydc(Ce). In addition, the inductively coupled plasma-mass spectroscopy (ICP-MS) show that the Zn/Zr and Ce/Zr atom ratio are 0.20:1 and 0.15:1 in bpydc (Zn) or UiO-bpydc(Ce) respectively, lower than the theoretical value (1:1) if all the bpydc ligands coordinate with metal. The results may be explained as follows: once the bpydc ligand on the surface coordinates with metal, it will decrease the pore size and block the bpydc ligand inside the nanoparticles further coordinate with metal.

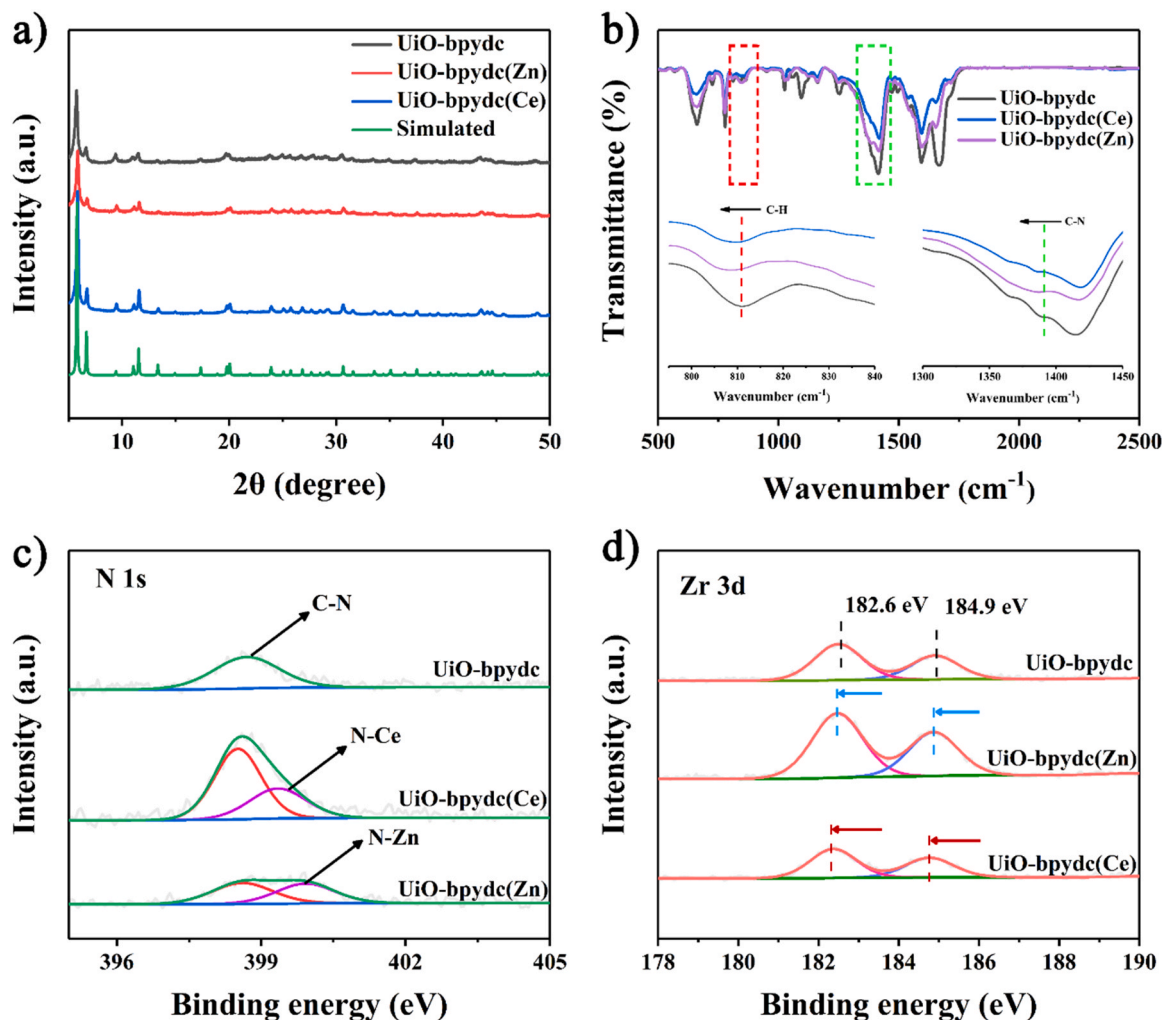**Scheme 1.** The synthetic procedure of UiO-bpydc(M), M=Ce or Zn.

Fig. 1. (a) XRD patterns and (b) FTIR spectra for UiO-bpydc, UiO-bpydc(Zn) and UiO-bpydc(Ce) (inset shows the magnified parts); XPS spectra for (c) N 1s and (d) Zr 3d of UiO-bpydc, UiO-bpydc(Zn) and UiO-bpydc(Ce).

In order to confirm the coordination environment of Zn and Ce in UiO-bpydc(M), Fourier transform infrared spectra (FTIR) and X-ray photoelectron spectra (XPS) were investigated. The FTIR spectra (Fig. 1b) suggest that the aromatic C-H stretching peak for the ligand bpydc in UiO-bpydc(Zn) (807 cm^{-1}) and UiO-bpydc(Ce) (808 cm^{-1}) shift to lower wavenumber compared with that for UiO-bpydc (810 cm^{-1}) [29]. Meanwhile, the stretching vibrational peak of C-N for bpydc in UiO-bpydc(Zn) (1386 cm^{-1}) or UiO-bpydc(Ce) (1386 cm^{-1}) also displays similar shift compared with UiO-bpydc (1390 cm^{-1}) [30]. The shift is most likely due to the Zn-N or Ce-N bond formation for UiO-bpydc(Zn) or UiO-bpydc(Ce) respectively. In

addition, no new peaks for the COO vibration can be detected, suggesting that Zn or Ce does not coordinate with the carboxylate group. The analysis of XPS spectra also suggest the successful coordination of Zr or Ce with bpydc. For the N 1 s spectra (Fig. 1c), a new peak at 399.4 eV for N-Zn of UiO-bpydc(Zn) and at 399.9 eV for N-Ce of UiO-bpydc(Ce) obviously appear compared with pristine UiO-bpydc,[31,32] implying that Ce or Zn successfully coordinates with the dipyridyl group in bpydc for UiO-bpydc(M). The Zr spectra (Fig. 1d) also show that the peak of Zr $3d_{1/2}$ and $3d_{3/2}$ for UiO-bpydc(M) display an obviously negative shift, compared with pristine UiO-bpydc (182.6 eV of $3d_{3/2}$ and 184.9 eV of $3d_{1/2}$) [33]. This result suggests that the Zn or Ce coordination leads to

an increase of electron density for the Zr cluster, which in turn reflects a fact that the Zn or Ce atom displays strong interaction with the bpydc, even the Zr cluster. The Zn 2p spectra (Fig. S1) obviously suggest the presence of Zn(II) in UiO-bpydc(Zn), with two peaks at 1021.6 and 1044.7 eV, belonging to the Zn $2p_{3/2}$ and Zn $2p_{1/2}$, respectively [34]. The Ce 3d spectra (Fig. S2) show that the Ce(IV) exists in UiO-bpydc(Ce), and the peaks at 881.7 and 885.8 eV are assigned to $3d_{5/2}$ and the ones at 900.1 and 904 eV to $3d_{3/2}$ [35].

Theoretical calculations based on density functional theory (DFT) were carried out in order to reveal the adsorption behavior for CO_2 and propylene oxide over the samples. Fig. S3a and S3b show the optimized configurations of UiO-bpydc and UiO-bpydc(Zn) [36,37]. As can be seen from Table 1, for UiO-bpydc, CO_2 tends to adsorb on the N of bpydc rather than Zr cluster, and propylene oxide tends to adsorb on the Zr cluster rather than the N in bpydc. Oppositely, for UiO-bpydc(Zn) and UiO-bpydc(Ce), CO_2 tends to adsorb on the Zr cluster, and propylene oxide prefers to adsorb on the Zn or Ce site instead of Zr cluster. These results suggest that, for pristine UiO-bpydc, Zr can be regarded as Lewis acid site and the N in bpydc as Lewis base site, which adsorb propylene oxide and CO_2 respectively. However, with the introduction of metal (Zn or Ce), which can also be regarded as Lewis acid, into the N in bipyridyl, the metal-N becomes Lewis acidic sites, and propylene oxide preferentially adsorbs on them rather than CO_2. Instead, CO_2 adsorbs on the Zr site (Fig. 2). Obviously, the introduction of Zn/Ce reverses the adsorption sites for CO_2 and propylene oxide.

The CO_2 adsorption capacity over the samples were also investigated. As shown in Fig. S4, UiO-bpydc(Zn) (62 cm^3/g) and UiO-bpydc (Ce) (68 cm^3/g) display decreased maximum CO_2 amount, compared with UiO-bpydc (71 cm^3/g). The specific BET (Brunner−Emmet−Teller) surface area (Fig. S5) suggests an opposite trend, namely, UiO-bpydc displays much larger BET value (2159 m^3g^{-1}) than the two counterparts (1827 m^3g^{-1} for UiO-bpydc(Zn) and 1815 m^3g^{-1} for UiO-bpydc (Ce)). It is reasonable that the BET surface area decreases for UiO-bpydc(M), as the introduction of metal would decrease the pore volume [38]. However, the CO_2 adsorption capacity per BET surface area for UiO-bpydc(Zn) or UiO-bpydc(Ce) is noticeably higher than that for UiO-bpydc (Fig. S6), suggesting that UiO-bpydc(Zn) and UiO-bpydc(Ce) display a significantly enhanced adsorption of CO_2. In other words, compared with UiO-bpydc, UiO-bpydc(Ce) and UiO-bpydc(Zn) with higher electronic density around Zr cluster are helpful to CO_2 adsorption [39].

3.2. Photocatalytic performance

As can be seen from Fig. 3a, the TON for UiO-bpydc(Zn) or UiO-bpydc(Ce) is higher than that for UiO-bpydc under dark condition, which are around 1.2 times and 1.4 times for UiO-bpydc(Ce) and UiO-bpydc(Zn) than that for UiO-bpydc respectively. Obviously, the introduction of Lewis acid (Zn or Ce ions) could efficiently increase the reaction rate. In addition, the TON for UiO-bpydc(Zn) is higher than that for UiO-bpydc(Ce) under dark condition, implying that Zn is more helpful for the ring opening of propylene oxide. Under light irradiation, the TON over UiO-bpydc, UiO-bpydc(Ce) and UiO-bpydc(Zn) all significantly increase (ca. 2.5 times, 2 times, 3.8 times compared with that under dark condition respectively), and UiO-bpydc(Zn) displays the

most prominent enhancement under light irradiation. Obviously, the light enhancement is dependent on the metal and the order is as follows: UiO-bpydc(Zn) > UiO-bpydc > UiO-bpydc(Ce). In other words, under light irradiation, the presence of Ce suppresses the reaction.

Control experiments suggest that UiO-bpydc(Zn) is an efficiency photocatalyst for the CO_2 cycloaddition reaction (Table S1). In addition, the influence of light and temperature on this reaction is further analyzed (Fig. S7). When the temperature increases, the TON over UiO-bpydc(Zn) improves slightly, which is consistent the accepted point that temperature is in favor of this reaction. Nevertheless, once introducing light into the system, the TON over UiO-bpydc(Zn) increases more obviously compared with the improvement induced by temperature. The TON over UiO-bpydc(Zn) is around 3 times under light irradiation than that under dark regardless of temperature. Meanwhile, the plot for TON vs wavelength is consistent with the absorption spectra of UiO-bpydc(Zn) (Fig. S8). Under ultraviolet light irradiation, the TON is close to the value under full spectrum light irradiation. When wavelength is longer than 420 nm, the TON is close to that under dark condition. Hence, it is safe to conclude that light displays more significant influence on this reaction compared with temperature. Moreover, the epoxide with other substituents were investigated (Table S2). To our delight, high conversion can be achieved for all the epoxides, indicating the great substrate tolerance of the catalyst.

UiO-bpydc(Zn) is proved to be stable via cycle experiments (Fig. S9). After six cycles tests, UiO-bpydc(Zn) still maintains excellent performance. The XRD spectra suggest no detectable difference before and after the stability test (Fig. S10). Besides that, the XPS spectra also show ignorable changes for UiO-bpydc(Zn) after the stability test, with respect to the N 1 s, Zr 3d and Zn 2p spectra (Fig. S11). All of the above results suggest the favorable stability of UiO-bpydc(Zn), which is very important to practical application. Most importantly, the performance of CO_2 cycloaddition over UiO-bpydc(Zn) is comparable with many other catalysts under mild conditions (Table S3). In addition, compared with the results obtained under high temperature and high pressure, our result over UiO-bpydc(Zn) is even better. Hence, UiO-bpydc(Zn) is further applied to scale up the production of cyclic carbonate using a large reactor containing 50 ml propylene oxide (Fig. S12). After 8 h, the reaction rate over UiO-bpydc(Zn) is 1.25 ml/h, which provides the possibility of industrial application.

3.3. Exploration of possible mechanism

In order to find the reason for above results, photocatalytic CO_2 reduction were carried out, which demonstrate that both UiO-bpydc and UiO-bpydc(Zn) can reduce CO_2 under light irradiation with CO as the main product (Fig. S13). However, either in the dark or in the absence of CO_2, nearly no CO can be detected, suggesting that the excited state of the photocatalysts can effectively activate CO_2. In addition, in-situ EPR spectra (Fig. S14) were carried out, and the results are consistent with previous results [40–42]. That is, light irradiation generates Zr^{3+} due to the photogenerated electron transfer from the bpydc(Zn) to Zr cluster, and the produced Zr^{3+} further activate CO_2 by transferring electron to the latter. The in-situ FTIR spectra provide direct evidence for the CO_2 activation under light irradiation. As can be seen from Fig. 3b, two obvious new peaks (1713 cm^{-1} and 1541.6 cm^{-1}) appear after light irradiation, which are attributed to the typical active species of CO_2 (CO_2*) [43–45].

Besides that, the photophysical properties for UiO-bpydc(Zn), UiO-bpydc(Ce) and UiO-bpydc were also studied. The UV–vis diffuse reflectance (DRS) spectra (Fig. S15) show that UiO-bpydc(M) display a slightly red shift in the absorption edge compared with UiO-bpydc, which is not regarded as the main factor for the large different reaction rate. Hence, the steady and time-resolved photoluminescence (PL) spectra were further investigated. As presented in Fig. S16a, UiO-bpydc demonstrates a high PL intensity, due to the quick carrier recombination and the PL intensity is quenched for UiO-bpydc(M), suggesting that the
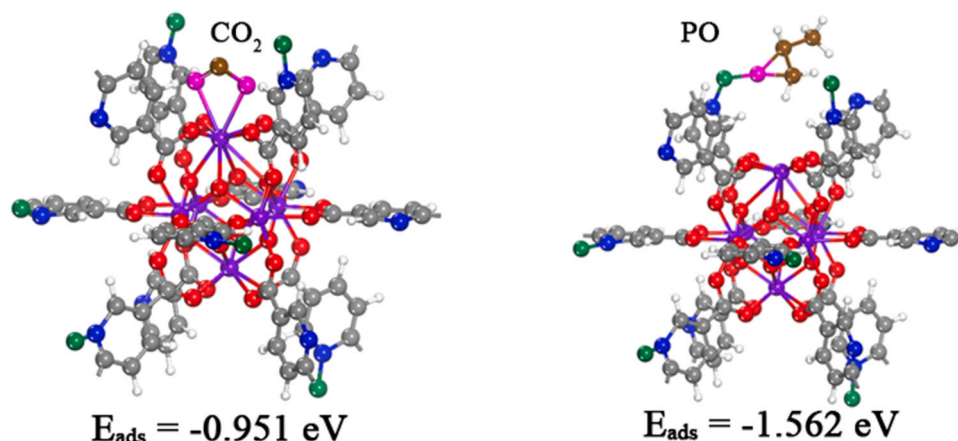
Table 1

Adsorption energy of CO_2 and propylene oxide on different sites in UiO-bpydc, UiO-bpydc(Zn) and UiO-bpydc(Ce) based on DFT calculations.

		CO_2	Epoxide
UiO-bpydc	N	-0.466 eV	-0.459 eV
	Zr	-0.352 eV	-0.897 eV
UiO-bpydc(Ce)	Ce	-0.667 eV	-1.971 eV
	Zr	-1.085 eV	-1.695 eV
UiO-bpydc(Zn)	Zn	-0.577 eV	-1.562 eV
	Zr	-0.951 eV	-0.875 eV

Fig. 2. The optimized structure after adsorption of CO_2 on Zr site (left) and propylene oxide on Zn site (right) over UiO-bpydc(Zn). Gray, red, purple, white, blue and green represent C, O, Zr, H, N and Zn over UiO-bpydc(Zn) respectively.
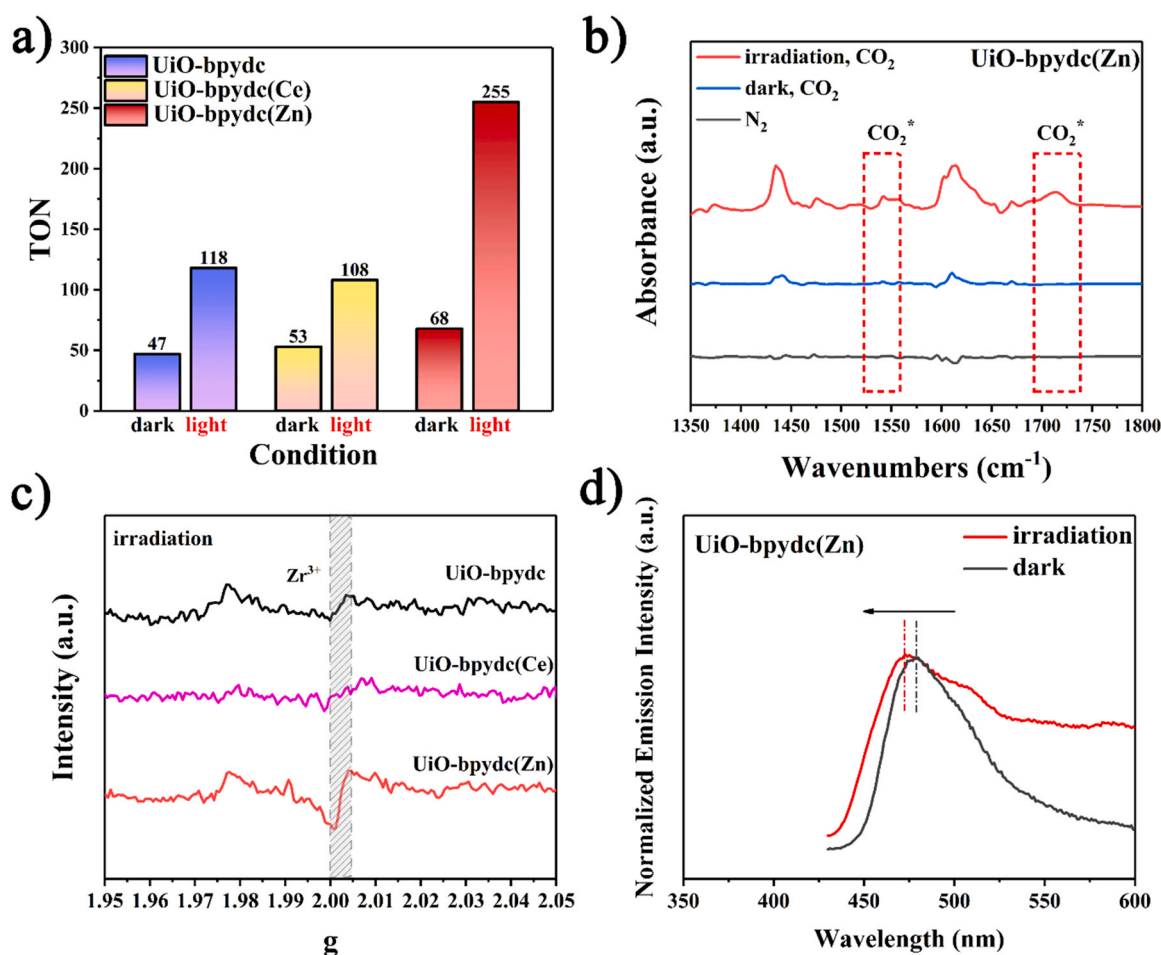

Fig. 3. (a) TON of CO_2 cycloaddition reaction under light illumination over UiO-bpydc, UiO-bpydc(Ce) and UiO-bpydc(Zn); (b) in situ FTIR spectra of UiO-bpydc(Zn) under different conditions; (c) in situ EPR spectra of Zr^{3+} signal over UiO-bpydc, UiO-bpydc(Ce) and UiO-bpydc(Zn) under light irradiation; (d) fluorescence spectra of NMA binding to UiO-bpydc(Zn) before and after irradiation in MeCN at 298 K.

introduction of Zn or Ce can effectively retard the carrier recombination. For time-resolved PL spectra (Fig. S16b), the average lifetime (τ) for UiO-bpydc(Zn) is 1.37 ns, longer than that for UiO-bpydc (1.23 ns). However, UiO-bpydc(Ce) displays a much shorter lifetime (0.38 ns) than does UiO-bpydc, implying that the decay path for the excited UiO-bpydc (Ce) may be different from that for UiO-bpydc and UiO-bpydc(Zn). According to our previous results [26], the introduction of Ce is beneficial

for energy transfer, which is competing to the widely accepted LMCT process. The overlap of the Ce-bpydc absorption and bpydc emission spectra (Fig. S17) justifies that the energy transfer would occur from the excited bpydc to Ce-bpydc [46–48].

The analysis of in-situ EPR spectra (Fig. 3c) confirm the energy transfer process as well. Under light irradiation, the signal of Zr^{3+} for UiO-bpydc(Ce) is weaker than that for UiO-bpydc, suggesting that the

LMCT process for the former is not as efficient as that for the latter, which is most likely due to the energy transfer process. UiO-bpydc(Zn) displays the strongest Zr^{3+} signal, implying that the introduction of Zn promotes the LMCT process, which are beneficial to activate CO_2.

N-methylacridone (NMA) fluorescence spectra were further investigated to verify the different photophysical properties with the introduction of different metals [49,50]. NMA is a commercially available fluorescent dye, which features lone pairs that can effectively bind to vacant Zr sites. The maximum fluorescence emission (λ_{max}) of NMA (433 nm) (Fig. S18) is sensitive to the binding affinity between NMA and Zr. Specifically, higher electron density leads to smaller binding affinity, which in turn shifts λ_{max} towards short wavelength. In dark, the λ_{max} for the three catalysts are as follows: 480 nm for UiO-bpydc, 478 nm for UiO-bpydc(Zn) and 473 nm for UiO-bpydc(Ce). The blue shift for UiO-bpydc(M) suggest increased electron density of Zr cluster, which is consistent with the XPS analysis. For UiO-bpydc(Zn), the λ_{max} changes dramatically from 478 nm to 472 nm under irradiation (Fig. 3d), suggesting the efficient photogenerated electron transfer from bpydc(Zn) to Zr. Most importantly, the light irradiation induced λ_{max} shift for UiO-bpydc(Zn) is the most prominent, further suggesting the effect of Zn in promoting the LMCT process.(Fig. S19a and S19b) When the λ_{max} under light irradiation is compared, NMA over UiO-bpydc(Ce) displays the shortest emission wavelength. This is because the introduction of Ce inhibits the LMCT process, and instead, energy transfer from bpydc to Ce-bpydc dominates the photophysical process. This is consistent with the EPR and PL spectra. Based on above results and discussion, the following conclusions can be obtained. The introduction of Zn into UiO-bpydc plays two significant roles: (1) promoting the LMCT process, which is beneficial for CO_2 activation; (2) enhancing the Lewis acidity, which is advantageous for the propylene oxide ring-opening.

4. Conclusion

In summary, Zn or Ce is successfully introduced into UiO-bpydc to obtain UiO-bpydc(M) to obtain UiO-bpydc(M), M=Zn or Ce. The effect of metal on the CO_2 cycloaddition efficiency is systematically investigated with respect to CO_2 and propylene oxide activation. This results suggest that UiO-bpydc(Zn) displays an optimized result, as introduction of Zn can not only activate propylene oxide effectively, but also promote the LMCT process, which leads to efficient CO_2 activation. This work proves that both the Lewis acidity and the photogenerated charge separation efficiency should be considered to achieve an optimal efficiency, which may provide guidance for further designing efficient photocatalysts for CO_2 cycloaddition.

CRediT authorship contribution statement

Guangyao Zhai: Methodology, Investigation, Formal analysis, Data curation, Writing - original draft. **Yuyin Mao**: Resources, Validation, Data curation. **Honggang Zhang**, **Lingtong Lin** and **Yujie Li**: Resources. **Zeyang Wang**, **Hefeng Cheng**, **Peng Wang** and **Zhaoke Zheng**: Resources, Project administration. **Yuanyuan Liu**, **Ying Dai** and **Biaobai Huang**: Conceptualization, Writing - review & editing.

Declaration of Competing Interest

The authors declare that they have no known competing financial interests or personal relationships that could have appeared to influence the work reported in this paper.

Acknowledgements

Appendix A. Supporting information

References

[1] L. Wan, Q. Zhou, X. Wang, T. Wood, L. Wang, P. Duchesne, J. Guo, X. Yan, M. Xia, Y. Li, A. Jelle, U. Ulmer, J. Jia, T. Li, W. Sun, G. Ozin, Cu₂O nanocubes with mixed oxidation-state facets for (photo)catalytic hydrogenation of carbon dioxide, Nat. Catal. 2 (2019) 889–898.

[2] Y. Gao, Q. Wu, X. Liang, Z. Wang, Z. Zheng, P. Wang, Yn Liu, Y. Dai, M. Whangbo, B. Huang, Cu₂O Nanoparticles with both {100} and {111} facets for enhancing the selectivity and activity of CO₂ electroreduction to ethylene, Adv. Sci. 7 (2020), 1902820.

[3] Q. Wang, D. Astruc, State of the art and prospects in metal−organic framework (MOF) based and MOF-derived nanocatalysis, Chem. Rev. 120 (2020) 1438–1511.

[4] Y. An, Y. Liu, P. An, J. Dong, B. Xu, Y. Dai, X. Qin, X. Zhang, M. Whangbo, B. Huang, Ni(II) coordination to an Al-based metal-organic framework made from 2-aminoterephthalate for photocatalytic overall water splitting, Angew. Chem. Int. Ed. (2017) 3036–3040.

[5] P. Zhou, G. Zhai, X. Lv, Y. Liu, Z. Wang, P. Wang, Z. Zheng, H. Cheng, Y. Dai, B. Huang, Boosting the electrocatalytic HER performance of Ni₃N-V₂O₃ via the interface coupling effect, Appl. Catal. B: Environ. 283 (2021), 119590.

[6] Y. Liu, Y. Yang, Q. Sun, Z. Wang, B. Huang, Y. Dai, X. Qin, X. Zhang, Chemical adsorption enhanced CO₂ capture and photoreduction over a copper porphyrin based metal organic framework. ACS Appl. Mater. Interfaces 5 (2013) 7654–7658.

[7] M. Mikkelsen, M. Jørgensen, F.C. Krebs, A review of fixation and transformation of carbon dioxide, Energy Environ. Sci. 3 (2010) 43–81.

[8] Y. Guo, B. Gao, Z. Deng, Y. Liu, X. Peng, Y. Zhao, Charge separation in hybrid metal–organic framework films for enhanced catalytic CO₂ conversion, J. Mater. Chem. A 9 (2021) 2694–2699.

[9] D. Tian, B. Liu, Q. Gan, H. Li, D. Darensbourg, Formation of cyclic carbonates from carbon dioxide and epoxides coupling reactions efficiently catalyzed by robust, recyclable one-component aluminum-salen complexes, ACS Catal. 2 (2012) 2029–2035.

[10] Q. Yang, C. Yang, C. Lin, H. Jiang, Metal–organic-framework-derived hollow N-doped porous carbon with ultrahigh concentrations of single Zn atoms for efficient carbon dioxide conversion, Angew. Chem. 131 (2019) 3549–3553.

[11] M. North, R. Pasquale, Mechanism of cyclic carbonate synthesis from epoxides and CO₂, Angew. Chem., Int. Ed. 48 (2009) 2946–2948.

[12] M. Ding, R.W. Flaig, H.L. Jiang, O.M. Yaghi, Carbon capture and conversion using metal-organic frameworks and MOF-based materials, Chem. Soc. Rev. 48 (2019) 2783–2828.

[13] D.J. Darensbourg, J.C. Yarbrough, C. Ortiz, C.C. Fang, Comparative kinetic studies of the copolymerization of cyclohexene oxide and propylene oxide with carbon dioxide in the presence of chromium salen derivatives. In situ FTIR measurements of copolymer vs cyclic carbonate production, J. Am. Chem. Soc. 125 (2003) 7586–7591.

[14] A. Decortes, A.M. Castilla, A.W. Kleij, Salen-complex-mediated formation of cyclic carbonates by cycloaddition of CO₂ to epoxides, Angew. Chem., Int. Ed. 49 (2010) 9822–9837.

[15] Y.Y. Zhang, G.W. Yang, R. Xie, L. Yang, B. Li, G.P. Wu, Scalable, durable, and recyclable metal-free catalysts for highly efficient conversion of CO₂ to cyclic carbonates, Angew. Chem. Int. Ed. 132 (2020) 2–10.

[16] G. Zhai, Y. Liu, L. Lei, J. Wang, Z. Wang, Z. Zheng, P. Wang, H. Cheng, Y. Dai, B. Huang, Light-promoted CO₂ conversion from epoxides to cyclic cCarbonates at ambient conditions over a Bi-based metal–organic framework, ACS Catal. 11 (2021) 1988–1994.

[17] M. Liu, F. Wang, L. Shi, L. Liang, J. Sun, Zn-based ionic liquids as highly efficient catalysts for chemical fixation of carbon dioxide to epoxides, RSC Adv. 5 (2015) 14277–17284.

[18] C. Chatterjee, M.H. Chisholm, The influence of the metal (Al, Cr, and Co) and the substituents of the porphyrin in controlling the reactions involved in the copolymerization of propylene oxide and carbon dioxide by porphyrin metal(III) complexes. 1. Aluminum chemistry, Inorg. Chem. 50 (2011) 4481–4492.

[19] C. Chatterjee, M.H. Chisholm, A. El-Khaldy, R.D. McIntosh, J.T. Miller, T. Wu, Influence of the metal (Al, Cr, and Co) and substituents of the porphyrin in controlling reactions involved in copolymerization of propylene oxide and carbon dioxide by porphyrin metal(III) complexes. 3. Cobalt chemistry, Inorg. Chem. 52 (2013) 4547–4553.

[20] G. Kresse, J. Furthmüller, Efficiency of ab-initio total energy calculations for metals and semiconductors using a plane-wave basis set, Comput. Mater. Sci. 6 (1996) 15–50.

[21] G. Kresse, J. Furthmüller, Efficient iterative schemes for ab initio total-energy calculations using a plane-wave basis set, Phys. Rev. B 54 (1996) 11169–11186.

[22] J. Perdew, P.K. Burke, M. Ernzerhof, Generalized gradient approximation made simple, Phys. Rev. Lett. 77 (1996) 3865–3868.

[23] G. Kresse, D. Joubert, From ultrasoft pseudopotentials to the projector augmented-wave method, Phys. Rev. B. 59 (1999) 1758–1775.

[24] P.E. Blöchl, Projector augmented-wave method, Phys. Rev. B 50 (1994) 17953–17979.

[25] S. Grimme, J. Antony, S. Ehrlich, H. Krieg, A consistent and accurate ab initio parametrization of density functional dispersion correction (DFT-D) for the 94 elements H-Pu, J. Chem. Phys. 132 (2010) 154104.

[26] Y. An, Y. Liu, H. Bian, Z. Wang, P. Wang, Z. Zheng, Y. Dai, M. Whangbo, B. Huang, Improving the photocatalytic hydrogen evolution of UiO-67 by incorporating Ce^{4+} coordinated bipyridinedicarboxylate ligands, Sci. Bull. 64 (2019) 1502–1509.

[27] T. Zhuo, Y. Song, G. Zhuang, L. Chang, S. Yao, W. Zhang, Y. Wang, P. Wang, W. Lin, T. Lu, Z. Zhang, H-bond-mediated selectivity control of formate versus CO during CO_2 photoreduction with two cooperative Cu/X sites, J. Am. Chem. Soc. 143 (2021) 6114–6122.

[28] J.B. DeCoste, G.W. Peterson, H. Jasuja, T.G. Glover, Y. Huang, K.S. Walton, Stability and degradation mechanisms of metal–organic frameworks containing the $Zr_6O_4(OH)_4$ secondary building unit, J. Mater. Chem. A 1 (2013) 5642–5650.

[29] A.E. Platero-Prats, A. Bermejo Gómez, L. Samain, X. Zou, B. Martín-Matute, The first one-pot synthesis of metal–organic frameworks functionalised with two transition-metal complexes, Chem. Eur. J. 21 (2015) 861–866, 861-566.

[30] Y. Song, D. Yang, S. Yu, X. Teng, Z. Chang, F. Pan, X. Bu, Z. Jiang, B. Wang, S. Wang, X. Cao, Hybrid membranes with Cu(II) loaded metal organic frameworks for enhanced desulfurization performance, Sep. Purif. Technol. 210 (2019) 258–267.

[31] S. Zhu, H. Yin, Y. Wang, K.S. Hui, X. Wu, W. Mai, X. Hong, F. Chen, K.N. Hui, Heteroatomic interface engineering of MOF-derived metal embedded P- and N-codoped Zn node porous polyhedral carbon with enhanced sodium-ion storage, ACS Appl. Energy Mater. 3 (2020) 8892–8902.

[32] L. Luo, L. Huang, X. Liu, W. Zhang, X. Yao, L. Dou, X. Zhang, Y. Nian, J. Sun, J. Wang, Mixed-valence Ce-BPyDC metal−organic framework with dual enzyme-like activities for colorimetric biosensing, Inorg. Chem. 58 (2019) 11382–11388.

[33] Y. Bai, Y. Dou, L.H. Xie, W. Rutledge, J.R. Li, H.C. Zhou, Zr-based metal–organic frameworks: design, synthesis, structure, and applications, Chem. Soc. Rev. 45 (2016) 2327–2367.

[34] F. Li, Y. Bu, G. Han, H. Noh, S. Kim, I. Ahmad, Y. Lu, P. Zhang, H.Y. Jeong, Z. Fu, Q. Zhong, J. Baek, Identifying the structure of Zn-N_2 active sites and structural activation, Nat. Commun. 10 (2019) 2623.

[35] A. López Cámara, V. Cortés Corberán, A. Martínez-Arias, L. Barrio, R. Si, J. C. Hanson, J.A. Rodriguez, Novel manganese-promoted inverse CeO_2/CuO catalyst: In situ characterization and activity for the water-gas shift reaction, Catal. Today 339 (2020) 24–31.

[36] M.I. Gonzalez, E.D. Bloch, J.A. Mason, S.J. Teat, J.R. Long, Single-crystal-to-single-crystal metalation of a metal−organic framework: a route toward structurally well-defined catalysts, Inorg. Chem. 54 (2015) 2995–3005.

[37] J. Hu, Y. Liu, J. Liu, C. Gu, D. Wu, High CO_2 adsorption capacities in UiO type MOFs comprising heterocyclic ligand, Microporous Mesoporous Mater. 256 (2018) 25–31.

[38] E.D. Bloch, D. Britt, C. Lee, C.J. Doonan, F.J. Uribe-Romo, H. Furukawa, J.R. Long, O.M. Yaghi, Metal insertion in a microporous metal-organic framework lined with 2,2′-bipyridine, J. Am. Chem. Soc. 132 (2010) 14382–14384.

[39] K. Megha, T.K. Mondal, A. Ghanty, A. Banerjee, Adsorption and activation of CO_2 on small-sized Cu−Zr bimetallic clusters, J. Phys. Chem. A 125 (2021) 2558–2572.

[40] D. Sun, Y. Fu, W. Liu, L. Ye, D. Wang, L. Yang, X. Fu, Z. Li, Studies on photocatalytic CO_2 reduction over NH_2-Uio-66(Zr) and its derivatives: towards a better understanding of photocatalysis on metal-organic frameworks, Chem Eur. J. 19 (2013) 14279–14285.

[41] D. Sun, W. Liu, M. Qiu, Y. Zhang, Z. Li, Introduction of a mediator for enhancing photocatalytic performance via post-synthetic metal exchange in metal-organic frameworks (MOFs), Chem. Commun. 51 (2015) 2056–2059.

[42] J. Long, S. Wang, Z. Ding, S. Wang, Y. Zhou, L. Huang, X. Wang, Amine-functionalized zirconium metal-organic framework as efficient visible-light photocatalyst for aerobic organic transformations, Chem. Commun. 48 (2012) 11656–11658.

[43] H. Wang, Q. Tang, Z. Wu, Construction of few-layer Ti_3C_2 MXene and boron-doped g-C3N4 for enhanced photocatalytic CO_2 reduction, ACS Sustain. Chem. Eng. 9 (2021) 8425–8434.

[44] R. Nakamura, A. Imanishi, K. Murakoshi, Y. Nakato, In situ FTIR studies of primary intermediates of photocatalytic reactions on nanocrystalline TiO_2 films in contact with aqueous solutions, J. Am. Chem. Soc. 125 (2003) 7443–7450.

[45] X. Li, L. Liang, Y. Sun, J. Xu, X. Jiao, X. Xu, H. Ju, Y. Pan, J. Zhu, Y. Xie, Ultrathin conductor enabling efficient IR light CO_2 reduction, J. Am. Chem. Soc. 141 (2019) 423–430.

[46] C.Y. Lee, O.K. Farha, B.J. Hong, A.A. Sarjeant, S.T. Nguyen, J.T. Hupp, Light-harvesting metal-organic frameworks (MOFs): efficient strut-to-strut energy transfer in bodipy and porphyrin-based MOFs, J. Am. Chem. Soc. 133 (2011) 15858–15861.

[47] J. Park, D. Feng, S. Yuan, H.C. Zhou, Photochromic metal–organic frameworks: reversible control of singlet oxygen generation, Angew. Chem. Int. Ed. 54 (2015) 430–435.

[48] K.E. Sapsford, L. Berti, I.L. Medintz, Materials for fluorescence resonance energy transfer analysis: beyond traditional donor–acceptor combinations, Angew. Chem. Int. Ed. 45 (2006) 4562–4588.

[49] P. Ji, X. Feng, P. Oliveres, Z. Li, A. Murakami, C. Wang, W. Lin, Strongly lewis acidic metal−organic frameworks for continuous flow catalysis, J. Am. Chem. Soc. 141 (2019) 14878–14888.

[50] P. Ji, T. Drake, A. Murakami, P. Oliveres, J.H. Skone, W. Lin, Tuning Lewis acidity of metal−organic frameworks via perfluorination of bridging ligands: spectroscopic, theoretical, and catalytic studies, J. Am. Chem. Soc. 140 (2018) 10553–10561.